Supramolecular assembly under the control of the chelating ligand for the Mn^{II}/bridging ligands/3-sulfobenzoate system and catalytic properties for the disproportionation of hydrogen peroxide†‡

Xiao-He Miao and Long-Guan Zhu*

Received (in Montpellier, France) 27th August 2009, Accepted 17th November 2009
DOI: 10.1039/b9nj00428a

Six Mn^{II} 3-sulfobenzoate complexes with neutral ligands, $[Mn(4,4'\text{-bipy})_2(H_2O)_4](3\text{-sb})\cdot 3H_2O$ (**1**), $\{[Mn(3\text{-sb})(bpe)_{1.5}(H_2O)_2](bpe)_{0.5}\cdot H_2O\}_n$ (**2**), $[Mn(3\text{-sb})(phen)(H_2O)_3](4,4'\text{-bipy})\cdot H_2O$ (**3**), $[Mn_2(3\text{-sb})_2(phen)_2\ (4,4'\text{-bipy})(H_2O)_4]$ (**4**), $[Mn(3\text{-sb})(phen)_2(H_2O)]\ (bpe)_{0.5}\cdot 4H_2O$ (**5**), and $[Mn(3\text{-sb})(phen)_2(H_2O)](bpe)_{0.5}\cdot H_2O$ (**6**) [where 3-sb is 3-sulfobenzoate, 4,4′-bipy is 4,4′-bipyridine, bpe is 1,2-bis(4-pyridine)ethylene, and phen is 1,10-phenanthroline], were synthesized and characterized by several modern analytic methods. The molecular structures for the six complexes are monomers for complexes **3**, **5**, and **6**, cation–anion species for complex **1**, dimer for complex **4**, and 1-D polymer for complex **2**. The phen ligands in complexes **3** and **4** generate some effects on the hydrogen-bonding network, π–π interactions, and supramolecular assembly. TG analysis showed that desolvated complexes containing 4,4′-bipy are less stable than those of complexes containing bpe ligands. The emission strength order is **1** > **5** > **6** > **3** > **2** > **4**, while the UV-vis absorption strengths are **4** > **3** > **1** for complexes containing 4,4′-bipy, and **5** > **6** > **2** for bpe metal complexes. The catalytic experiments showed that these six complexes are catalytically active for the disproportionation of H_2O_2 in the presence of imidazole and complex **3** has the best catalytic activity.

Introduction

Recently, 4,4′-bipyridine (4,4′-bipy) and 1,2-bis(4-pyridine) ethylene (bpe) ligands have widely been used as polymeric linkers for constructing fascinating coordination polymers in the field of potential functional materials.[1–5] The 4,4′-bipy or bpe ligands can also exhibit monodentate, dimeric linker or non-coordinating modes,[6–8] although they are relatively sparse. In previous studies, the 4,4′-bipy or bpe ligands in sulfobenzoate transition metal complexes gave novel coordination modes.[9–13] These studies focused on the ternary complexes with one neutral ligand. The coordination of neutral ligands with metal centers can largely change the coordination environments, resulting in the tuning of the properties. Therefore, we introduced the chelating ligand, 1,10-phenanthroline (phen), into the Mn^{II}/bridging ligands/sulfobenzoate system to investigate the influence of the mixed neutral ligands on the diverse topology and supramolecular assembly. On the other hand, Mn^{II} complexes have shown that they can act as catalysts in several reactions, such as epoxidation,[14] oxidative aromatization,[15] and oxidative decarboxylation.[16] Herein, we present the syntheses, crystal structures, and catalytic activity of six complexes based on the Mn^{II}/3-sulfobenzoate (3-sb) system with neutral N-donor ligands, $[Mn(4,4'\text{-bipy})_2(H_2O)_4](3\text{-sb})\cdot 3H_2O$ (**1**), $\{[Mn(3\text{-sb})(bpe)_{1.5}(H_2O)_2](bpe)_{0.5}\cdot H_2O\}_n$ (**2**), $[Mn(3\text{-sb})(phen)(H_2O)_3](4,4'\text{-bipy})\cdot H_2O$ (**3**), $[Mn_2(3\text{-sb})_2(phen)_2(4,4'\text{-bipy})(H_2O)_4]$ (**4**), $[Mn(3\text{-sb})(phen)_2(H_2O)](bpe)_{0.5}\cdot 4H_2O$ (**5**), and $[Mn(3\text{-sb})(phen)_2(H_2O)](bpe)_{0.5}\cdot H_2O$ (**6**).‡

Department of Chemistry, Zhejiang University, Hangzhou 310027, People's Republic of China. E-mail: chezlg@zju.edu.cn; Fax: 86-571-87951895; Tel: 86-571-87963867

† This article is part of a themed issue on Coordination polymers: structure and function.

‡ CCDC reference numbers 745965–745970. For crystallographic data in CIF or other electronic format see DOI: 10.1039/b9nj00428a

Results and discussion

Synthesis

Ternary complexes **1** and **2** showed that the 4,4′-bipy or bpe can act as a terminal or dimeric bridge linker; such coordination modes have been reported in our lab in the Mn^{II}/4-sb/4,4′-bipy system.[9a] The introduction of the second neutral ligand, phen, into the Mn^{II}/3-sb/4,4′-bipy or Mn^{II}/3-sb/bpe system can influence the coordination modes of 3-sb, 4,4′-bipy or bpe. The diverse coordination modes provide different and abundant supramolecular building blocks. Therefore complexes **3–6** were synthesized by using a two-step strategy.

The different synthetic conditions for complexes **3** and **4** are that reflux was used for synthesizing complex **3** while hydrothermal conditions were used for synthesizing complex **4**. Furthermore, the mixed solvents of H_2O–C_2H_5OH–DMF were used in the synthesis of complex **3**, while solvents of water and DMF were used in the synthesis of complex **4**. The synthetic methods and conditions for complexes **5** and **6** are similar to those in the syntheses of complexes **3** and **4**, respectively.

All these complexes are soluble in methanol and DMSO, but insoluble in H_2O, acetonitrile, and CH_2Cl_2.

Descriptions of crystal structures

[Mn(4,4′-bipy)$_2$(H$_2$O)$_4$](3-sb)·3H$_2$O(1). The X-ray analysis revealed that complex **1** is a cation–anion species consisting of a [Mn(4,4′-bipy)$_2$(H$_2$O)$_4$]$^{2+}$ cation, a 3-sb^{2-} anion, and lattice water molecules (Fig. 1 and Table 1). There are two kinds of metal environments but with similar geometrical parameters in complex **1** and these Mn ions lie on inversion centres. Each metal center is six-coordinated by four O atoms from four water molecules and two N donors from two 4,4′-bipy ligands. All observed Mn–O and Mn–N distances in **1** are similar to those reported in ref. 9*a*. The motif [Mn(4,4′-bipy)$_2$(H$_2$O)$_4$] has been found in several papers,[5,17] in which the 4,4′-bipy acts as a terminal ligand, monodentate mode. The pyridine rings of the 4,4′-bipy are not coplanar, with the dihedral angles of 19.29(6)° for Mn1 motif and 23.97(6)° for Mn2 motif, respectively. The [Mn(4,4′-bipy)$_2$(H$_2$O)$_4$] motif is a good hydrogen-bonding donor or acceptor, in which not only the water molecules but also the 4,4′-bipy ligands are capable of forming hydrogen-bonding interactions. The cations, [Mn(4,4′-bipy)$_2$(H$_2$O)$_4$]$^{2+}$, form 2-D hydrogen-bonding layers by hydrogen bonds between monodentate 4,4′-bipy ligands and coordinated water molecules (Fig. 2). Within the 2-D hydrogen-bonding layers, π–π interactions between 4,4′-bipy ligands occur with the centroid to centroid distances ranging from 3.570(2) Å to 3.784(2) Å.

The anions and lattice water molecules also form 2-D hydrogen-bonding layers (Fig. 3). The whole molecular structure is a 3-D

Table 1 Selected bond lengths (Å) and angles (°) in complex **1**

Mn1–O1	2.251(3)	Mn1–O2	2.177(3)
Mn1–N1	2.171(3)	Mn2–O3	2.299(3)
Mn2–O4	2.139(3)	Mn2–N3	2.180(3)
O1–Mn1–O2	88.69(13)	O1–Mn1–N1	87.44(12)
O2–Mn1–N1	88.78(12)	O3–Mn2–O4	90.42(15)
O3–Mn2–N3	94.46(14)	O4–Mn2–N3	90.42(15)

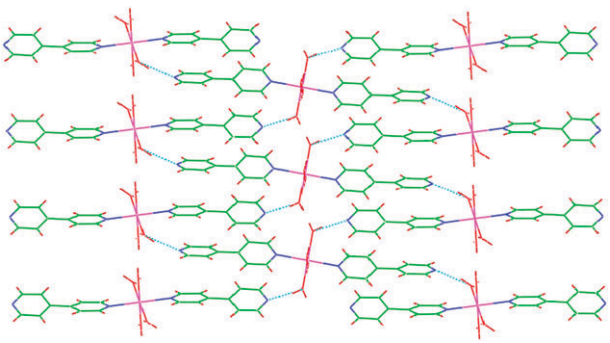

Fig. 2 View of 2-D hydrogen-bonding layer formed by cations in complex **1**.

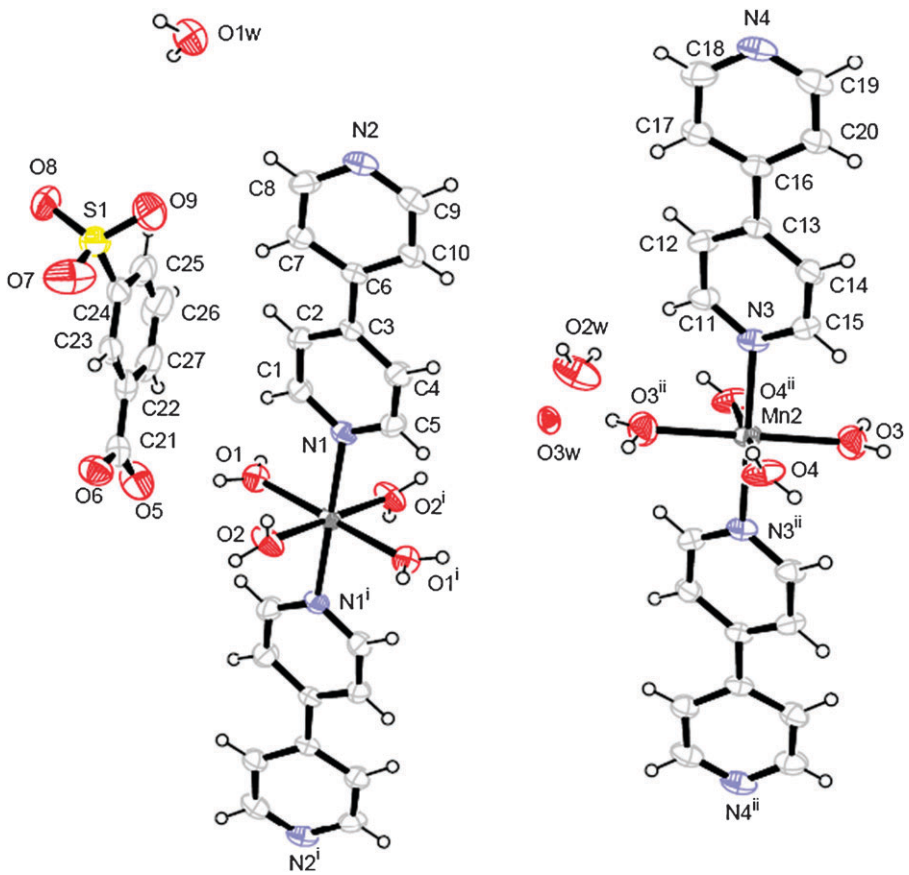

Fig. 1 View of the molecular structure of complex **1**. The thermal ellipsoids are drawn at 40% probability. Symmetry codes: i = −*x*, −*y*, −*z*; ii = 1 − *x*, −*y*, −*z*.

architecture assembled by hydrogen bonds and π–π interactions (Fig. 4).

{[Mn(3-sb)(bpe)$_{1.5}$(H$_2$O)$_2$](bpe)$_{0.5}$·H$_2$O}$_n$ (2). Each asymmetry unit of complex **2** contains one [Mn(3-sb)(bpe)$_{1.5}$(H$_2$O)$_2$] unit, half an uncoordinated bpe ligand, and one lattice water molecule

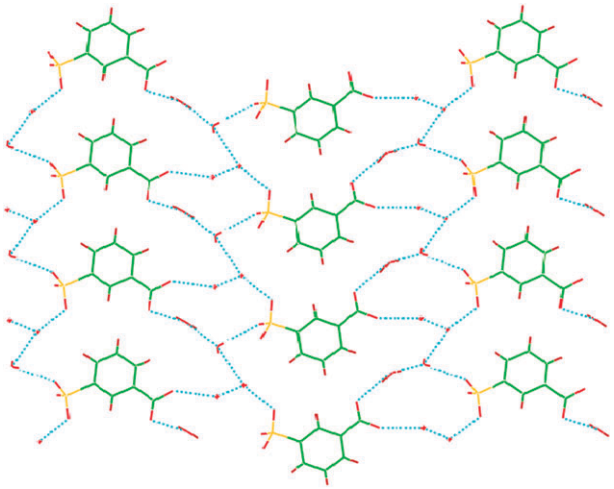

Fig. 3 View of 2-D layer formed by the anions and lattice water molecules in complex **1**.

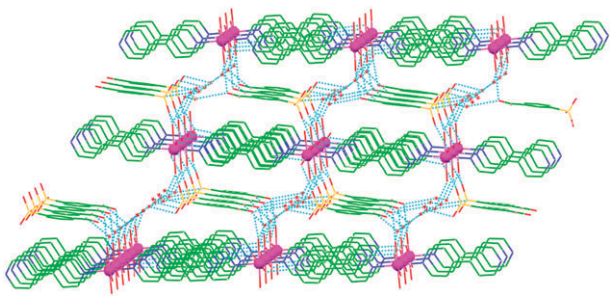

Fig. 4 View of the 3-D hydrogen-bonding architecture for complex **1**.

(Fig. 5 and Table 2). The metal center geometry is defined by six atoms forming a distorted octahedron. The 3-sb ligand bridges two Mn^{II} centers through two carboxyl oxygen atoms, while the sulfonate group is non-coordinating. The bpe ligands in complex **2** exhibit three coordination or existing modes, non-coordinating as a free ligand, dimeric bridge, monodentate and two bpe ligands (the bpe containing N3 and N4, respectively) lie about the inversion centres. Two pyridine rings in each bpe are nearly coplanar. The dimeric bridge mode of the bpe and the bridge coordination of the 3-sb result in the 1-D molecular structure (Fig. 6). The [Mn(3-sb)(bpe)$_{1.5}$(H$_2$O)$_2$] units assemble into a 2-D hydrogen-bonding layer by monodentate bpe and coordinated water molecules (Fig. 7).

The [Mn(3-sb)(bpe)$_{1.5}$(H$_2$O)$_2$] units and lattice water molecules form a 3-D hydrogen-bonding architecture with a 334.2 Å^3 hole, therefore the free ligands can occupy these holes (Fig. 8). The weak π–π interactions occur between dimeric linking bpe and monodentate bpe with the centroid-to-centroid distance of 3.914(3) Å, and between non-coordinating bpe ligands with the centroid-to-centroid distance of 3.891(3) Å.

[Mn(3-sb)(phen)(H$_2$O)$_3$](4,4′-bipy)·H$_2$O (3). Each repeat unit of complex **3** consists of one [Mn(phen)(3-sb)(H$_2$O)$_3$]

Table 2 Selected bond lengths (Å) and angles (°) in complex **2**

Mn1–O1	2.106(2)	Mn1–O2^i	2.133(2)
Mn1–O6	2.262(2)	Mn1–O7	2.181(2)
Mn1–N1	2.286(3)	Mn1–N3	2.254(3)
O1–Mn1–O2^i	112.14(9)	O1–Mn1–O6	89.51(9)
O1–Mn1–O7	169.65(9)	O1–Mn1–N1	88.04(10)
O1–Mn1–N3	85.39(10)	O2^i–Mn1–O6	157.08(9)
O2^i–Mn1–O7	78.10(9)	O2^i–Mn1–N1	92.61(10)
O2^i–Mn1–N3	90.26(10)	O6–Mn1–O7	80.56(9)
O6–Mn1–N1	95.70(9)	O6–Mn1–N3	83.84(9)
O7–Mn1–N1	90.03(11)	O7–Mn1–N3	96.36(11)
N1–Mn1–N3	173.41(10)		

Symmetry code, i: 1 − x, 2 − y, 1 − z.

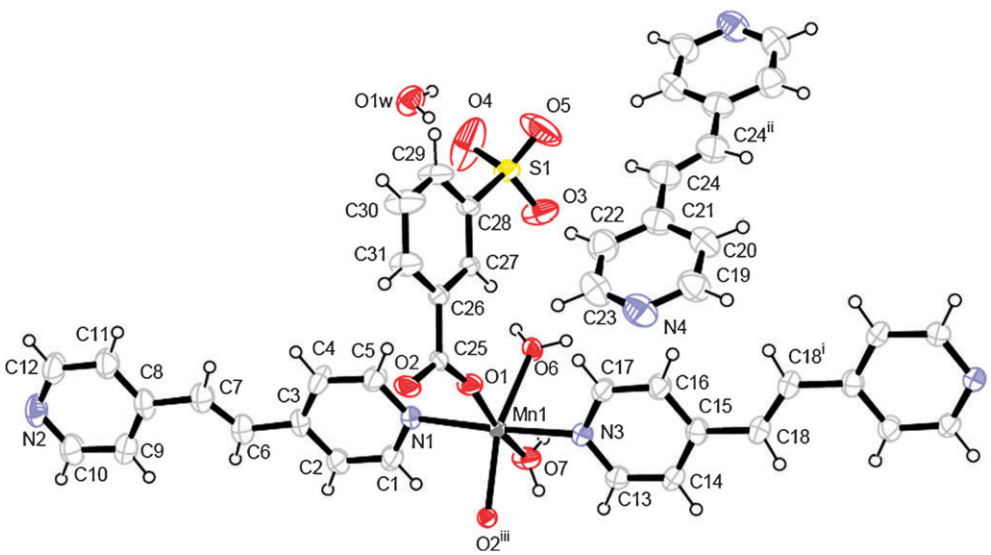

Fig. 5 View of the molecular structure of complex **2**. The thermal ellipsoids are drawn at 40% probability. Symmetry codes: i = 2 − x, 1 − y, 2 − z; ii = 2 − x, 2 − y, 2 − z; iii = 1 − x, 2 − y, 1 − z.

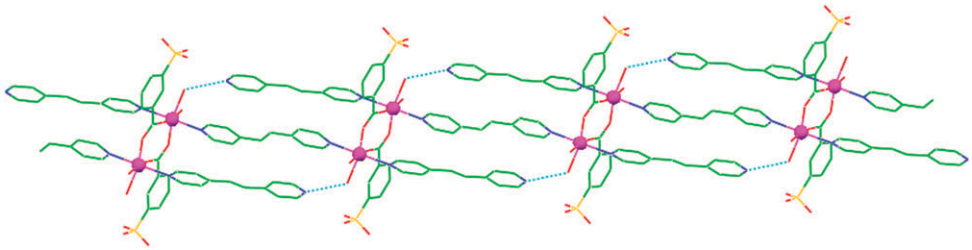

Fig. 6 View of the 1-D chain formed by $[Mn(3\text{-sb})(bpe)_{1.5}(H_2O)_2]$ units in complex **2**.

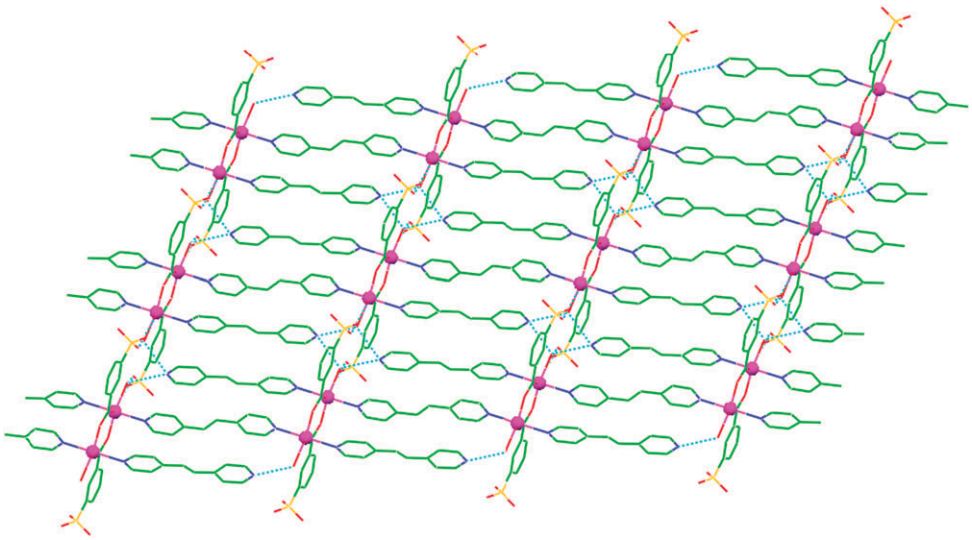

Fig. 7 View of the 2-D hydrogen-bonding layer formed by $[Mn(3\text{-sb})(bpe)_{1.5}(H_2O)_2]$ units in complex **2**.

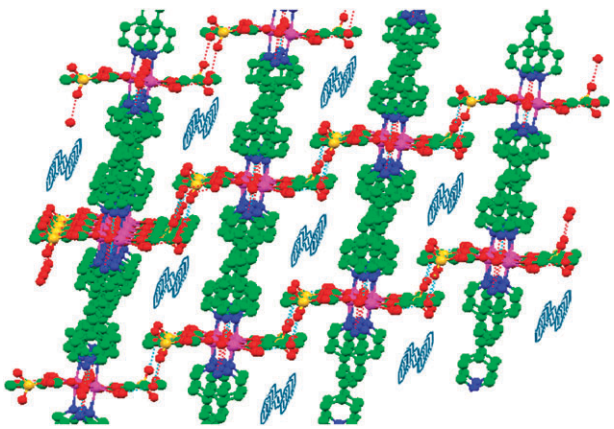

Fig. 8 View of the 3-D host–guest architecture for complex **2**. The stacked bpe ligands occupy the 3-D holes.

unit, one non-coordinating 4,4′-bipy, and one lattice water molecule. Each Mn^{II} center is coordinated by six coordination donors, two N donors from one phen, and four O atoms from three water molecules and one 3-sb ligand (Fig. 9 and Table 3). The 3-sb ligand is monodentately coordinated to the Mn^{II} center by the carboxyl group. The 4,4′-bipy ligand is non-coordinating, but forms hydrogen bonds with lattice water molecules and coordinated water molecules. The $[Mn(3\text{-sb})(phen)(H_2O)_3]$ units form a 2-D hydrogen-bonding layer (Fig. 10). The 2-D hydrogen-bonding layer of $[Mn(3\text{-sb})(phen)(H_2O)_3]$ units hold together into a 3-D architecture by lattice water molecules and 4,4′-bipy ligands (Fig. 11). Within the 3-D network, π–π interactions only between phen and bpe ligands with the centroid-to-centroid distances ranging from 3.625(2) Å to 3.7018(19) Å are observed.

$[Mn_2(3\text{-sb})_2(phen)_2(4,4'\text{-bipy})(H_2O)_4]$ (4). The molecular structure of complex **4** is a dimer. The geometry of each Mn^{II} can be described as a distorted octahedron completed by three N donors from one phen and one 4,4′-bipy and three O atoms from one 3-sb and two water molecules (Fig. 12 and Table 4). The 4,4′-bipy lies about an inversion centre and bridges two Mn^{II} centers as a dimeric linker. Pyridine rings of each 4,4′-bipy are wholly coplanar. The Mn···Mn separation by the 4,4′-bipy ligand is 11.618 Å. The inter-molecular hydrogen-bonding architecture is a 3-D network (Fig. 13), in which neighboring dimeric molecules contain π–π interactions only between phen ligands with the centroid-to-centroid distance of 3.6432(18) Å.

$[Mn(3\text{-sb})(phen)_2(H_2O)](bpe)_{0.5}\cdot 4H_2O$ (5). Complex **5** is made up of one $[Mn(3\text{-sb})(phen)_2(H_2O)]$ motif, half a free bpe which lies about an inversion centre and four lattice water molecules (Fig. 14 and Table 5). Each Mn^{II} center is six-coordinated by four N donors from two phen ligands and two O atoms from one 3-sb and one water molecule. Two phen ligands are nearly perpendicular to each other, with

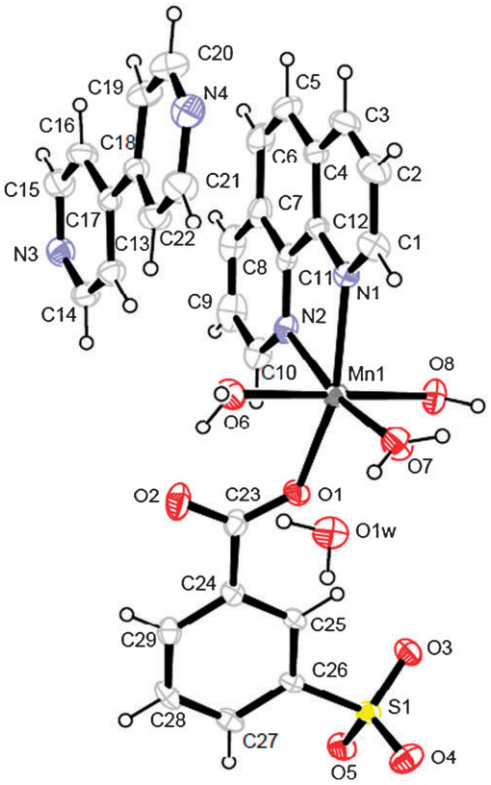

Fig. 9 View of the molecular structure of complex **3**. The thermal ellipsoids are drawn at 30% probability.

Table 3 Selected bond lengths (Å) and angles (°) in complex **3**

Mn1–O1	2.1311(18)	Mn1–O6	2.1924(18)
Mn1–O7	2.149(2)	Mn1–O8	2.1661(19)
Mn1–N1	2.291(2)	Mn1–N2	2.266(2)
O1–Mn1–O6	86.90(7)	O1–Mn1–O7	97.69(9)
O1–Mn1–O8	92.73(8)	O1–Mn1–N1	162.91(8)
O1–Mn1–N2	92.45(8)	O6–Mn1–O7	90.86(9)
O6–Mn1–O8	179.41(8)	O6–Mn1–N1	85.15(7)
O6–Mn1–N2	92.72(8)	O7–Mn1–O8	89.65(8)
O7–Mn1–N1	97.54(8)	O7–Mn1–N2	169.41(9)
O8–Mn1–N1	95.08(8)	O8–Mn1–N2	86.83(8)
N1–Mn1–N2	72.87(8)		

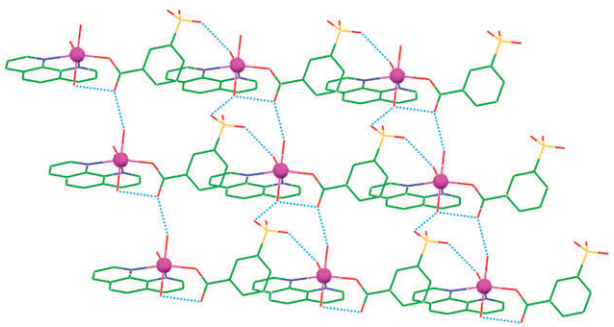

Fig. 10 View of the 2-D hydrogen-bonding layer formed by [Mn(3-sb)(phen)(H_2O)$_3$] units in complex **3**.

a dihedral angle of 82.7(1)° for rings C16–C19/C23–C24 and C5–C7/ C11–C12. The pyridine rings of the free bpe ligand are completely coplanar.

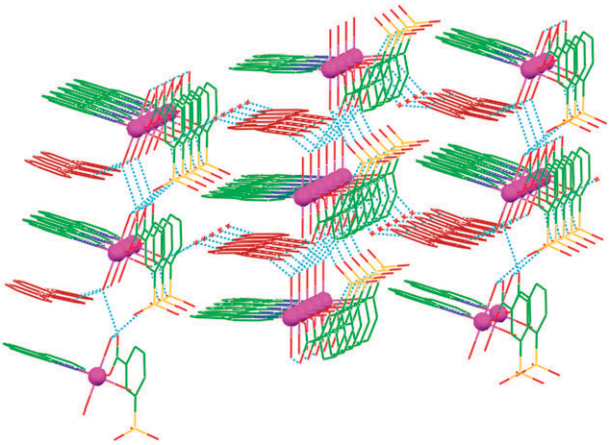

Fig. 11 View of the 3-D hydrogen-bonding network for complex **3**.

The [Mn(3-sb)(phen)$_2$(H_2O)] units form a 1-D hydrogen-bonding chain through the hydrogen bonds between the coordinated water molecule and sulfonate group (Fig. 15). The lattice water molecules and free bpe ligands form 2-D hydrogen-bonding layers (Fig. 16). The whole hydrogen-bonding network is a 3-D architecture (Fig. 17).

There are strong π–π interactions between phen ligands, and between phen and bpe ligands with the centroid-to-centroid distances ranging from 3.569(2) Å to 3.990(3) Å.

[Mn(3-sb)(phen)$_2$(H_2O)](bpe)$_{0.5}$·H_2O (6). The structure of complex **6** is similar to that of complex **5**, but they have different lattice water molecules (Fig. 18 and Table 6). The free bpe ligand lies about an inversion centre. Thus the hydrogen-bonding assembly and π–π interactions are different in complexes **5** and **6**.

The units [Mn(3-sb)(phen)$_2$(H_2O)] in complex **6** form hydrogen-bonding chains similar to those in complex **5**. In complex **5**, the bpe forms hydrogen bonds, while in complex **6**, the bpe does not form any hydrogen bonds.

The hydrogen-bonding structure of complex **6** is a 1-D chain (Fig. 19), which is very different from that of complex **5**. There are abundant π–π interactions in complex **6** between phen ligands, and between phen and bpe ligands with the centroid-to-centroid distances ranging from 3.5141(14) Å to 3.8864(18) Å.

Influence of phen on supramolecular assembly

The phen ligand coordinates to the metal center in a chelating mode, which reduces the coordination sites around the metal center; therefore the coordination of the phen can influence the molecular structure, hydrogen-bonding forming ability, and supramolecular assembly. Complexes **1** and **2** contain one neutral ligand, 4,4′-bipy or bpe, respectively, and the four complexes contain two neutral ligands, in which one of the neutral ligands is the phen. The 4,4′-bipy ligands exhibit a monodentate coordination mode and hydrogen-bonding forming ability in complex **1**, a free ligand but a hydrogen-bonding donor in complex **3**, and a dimeric linker in complex **4**. The bpe ligands show three modes in complex **2** (dimeric linker, monodentate, and free ligand), a free ligand as a hydrogen-bonding donor in complex **5**, and a free ligand without hydrogen-bonding forming ability in complex **6**. The different

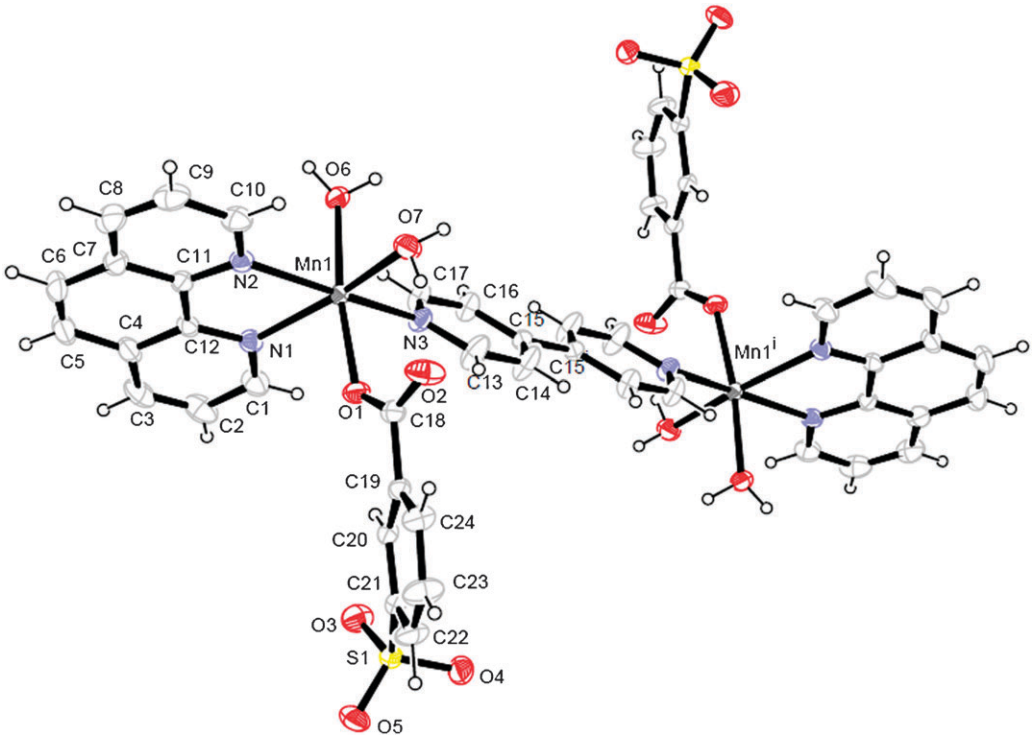

Fig. 12 View of the molecular structure for complex **4**. The thermal ellipsoids are drawn at 30% probability. Symmetry code: i = $-x$, $1-y$, $1-z$.

Table 4 Selected bond lengths (Å) and angles (°) in complex **4**

Mn1–O1	2.1143(16)	Mn1–O6	2.1694(18)
Mn1–O7	2.2001(19)	Mn1–N1	2.281(2)
Mn1–N2	2.269(2)	Mn1–N3	2.267(2)
O1–Mn1–O6	171.74(7)	O1–Mn1–O7	89.51(7)
O1–Mn1–N1	86.87(7)	O1–Mn1–N2	100.43(7)
O1–Mn1–N3	87.87(7)	O6–Mn1–O7	88.43(8)
O6–Mn1–N1	97.26(7)	O6–Mn1–N2	87.65(7)
O6–Mn1–N3	84.49(7)	O7–Mn1–N1	163.77(7)
O7–Mn1–N2	92.35(7)	O7–Mn1–N3	97.68(7)
N1–Mn1–N2	72.81(7)	N1–Mn1–N3	97.99(7)
N2–Mn1–N3	167.06(7)		

coordination modes for 4,4′-bipy in complexes **3** and **4**, and for bpe in complexes **5** and **6** compared with complexes **1** and **2** show that the phen ligands can adjust the coordination environments. The number of water molecules around the metal centers in 4,4-bipy complexes **3–4** and bpe complexes **5–6** are distinctly less than those corresponding 4,4′-bipy and bpe complexes **1** and **2**, respectively. Therefore, the introduction of the phen into the ternary metal systems largely changes the supramolecular assembles, resulting in the diverse topologies and different properties.

Thermal stability studies

The thermal decomposition behaviors of **1–6** were investigated in static air atmosphere from ambient to 800 °C. For the TG curve of complex **1** the first stage of weight loss occurred between 35 °C and 139 °C, corresponding to the removal of three lattice water molecules with the weight loss of 8.59% (calculated 8.96%). Further decomposition took place at 152 °C. Complex **2** lost water molecules from 61 to 146 °C with the weight loss of 8.14% (calculated 8.02%). Complex **2** decomposed at 172 °C. For complex **3**, the weight loss started at 73 °C and ended at 150 °C with the weight loss of 11.61% (calculated 10.86%). Complex **3** decomposed at 156 °C. Complex **4** lost water molecules from room temperature to 125 °C, with the weight loss of 6.47% (calculated 6.56%), and began to decompose at 137 °C. Complex **5** released water molecules from room temperature to 112 °C with the weight loss of 12.34% (calculated 11.28%). Complex **5** decomposed at 168 °C. Two-step release of lattice and coordinated water molecules were obviously observed from 70 °C to 141 °C with the weight loss of 5.41% (calculated 4.85%), and the complex **6** decomposed at 170 °C. For these six complexes, the residues are MnO_2 after 550 °C. To summarize, the TG curves showed that desolvated complexes **2**, **5**, and **6** are more stable than the others, indicating metal complexes containing 4,4′-bipy are less stable.

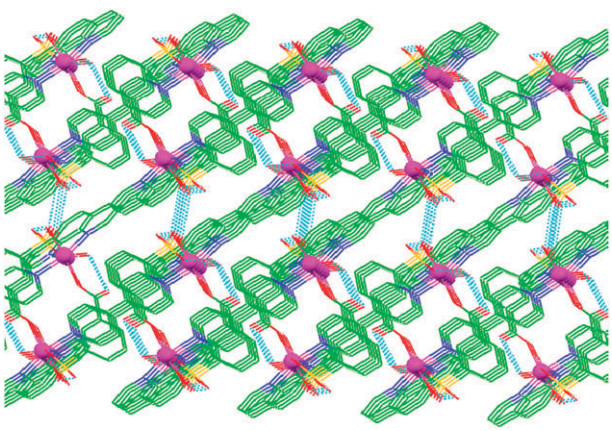

Fig. 13 View of 3-D hydrogen-bonding network for complex **4**.

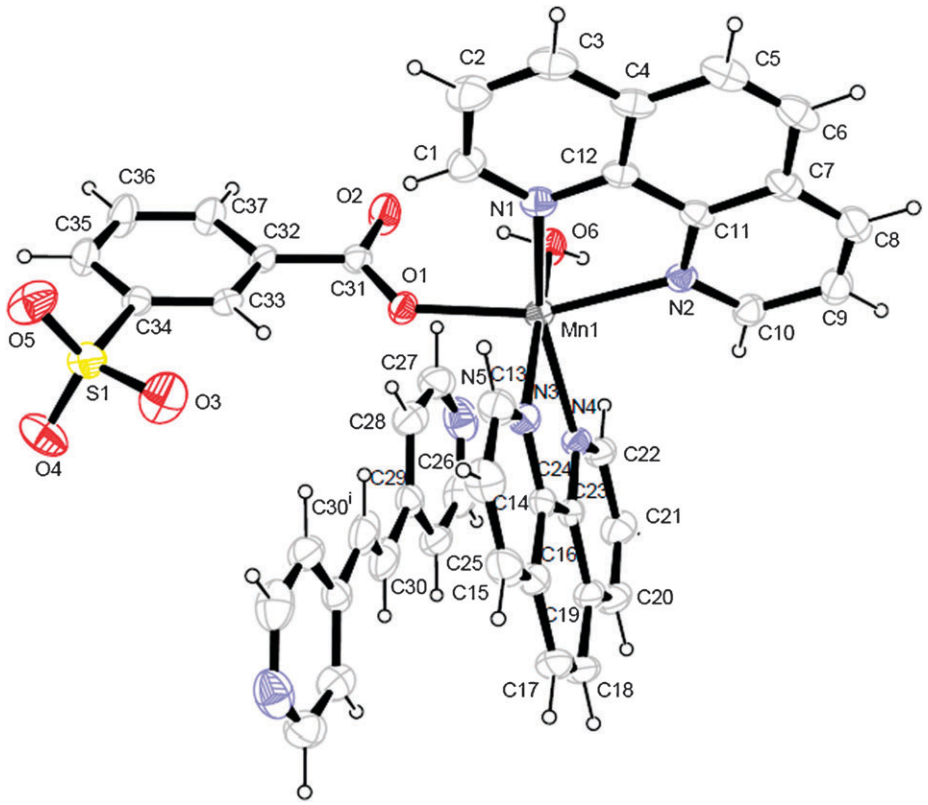

Fig. 14 View of the molecular structure for complex **5**. The thermal ellipsoids are drawn at 30% probability. Symmetry code: i = $1 - x, -y, 1 - z$. Lattice water molecules are omitted for clarity.

Table 5 Selected bond lengths (Å) and angles (°) in complex **5**

Mn1–O1	2.118(3)	Mn1–O6	2.148(3)
Mn1–N1	2.276(3)	Mn1–N2	2.279(3)
Mn1–N3	2.282(3)	Mn1–N4	2.272(3)
O1–Mn1–O6	89.66(11)	O1–Mn1–N1	91.07(11)
O1–Mn1–N2	162.40(11)	O1–Mn1–N3	89.31(10)
O1–Mn1–N4	105.11(10)	O6–Mn1–N1	103.28(14)
O6–Mn1–N2	87.91(12)	O6–Mn1–N3	166.09(14)
O6–Mn1–N4	94.10(13)	N1–Mn1–N2	72.57(12)
N1–Mn1–N3	90.61(12)	N1–Mn1–N4	156.36(12)
N2–Mn1–N3	97.13(11)	N2–Mn1–N4	92.45(11)
N3–Mn1–N4	72.80(12)		

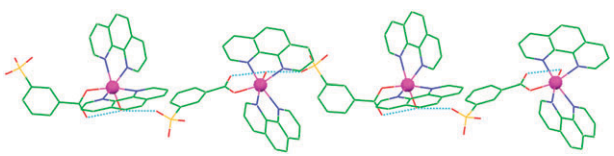

Fig. 15 View of the 1-D chain formed by $[Mn(3\text{-sb})(phen)_2(H_2O)]$ units in complex **5**.

Emission properties

The emission spectrum of **1** exhibits wondrously strong blue emissions compared to the others. The maximal peaks are 470.5 nm in **1**, 470.5 nm in **2**, 470.7 nm in **3**, 472.1 nm in **4**, 471.3 nm in **5**, and 471.4 nm in **6**, respectively. All these emissions mainly come from the 3-sb ligand,[18] which are more intense than the free 3-sb ligand. The emission strength order

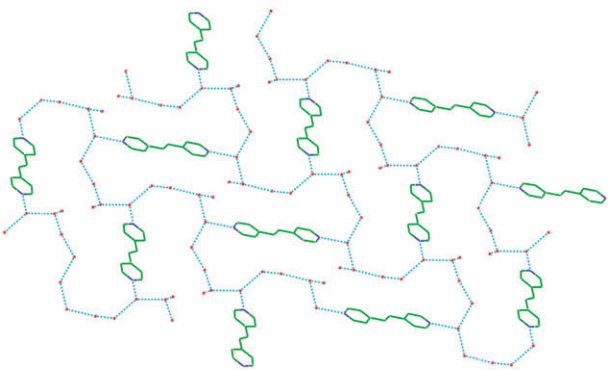

Fig. 16 View of the 2-D hydrogen-bonding layer formed by bpe and lattice water molecules in **5**.

is **1** > **5** > **6** > **3** > **2** > **4**. Therefore, in the 4,4′-bipy metal system the ternary metal complex, **1**, is strongest, while in the bpe metal system the ternary metal complex, **2**, is weakest.

Absorption spectra

These complexes have more intensive absorptions than those of free ligands, indicating that the coordination of ligands can enhance the absorption (Fig. 20 and Table 7). Complexes **1** and **2** with one 4,4′-bipy or bpe ligand possess relatively weaker absorption bands than the others with two neutral ligands. A slight blue-shift of absorption peaks for complex **1** belongs to LLCT type[19] compared with the free 4,4′-bipy ligand. On the contrary, complex **2** shows a complicated

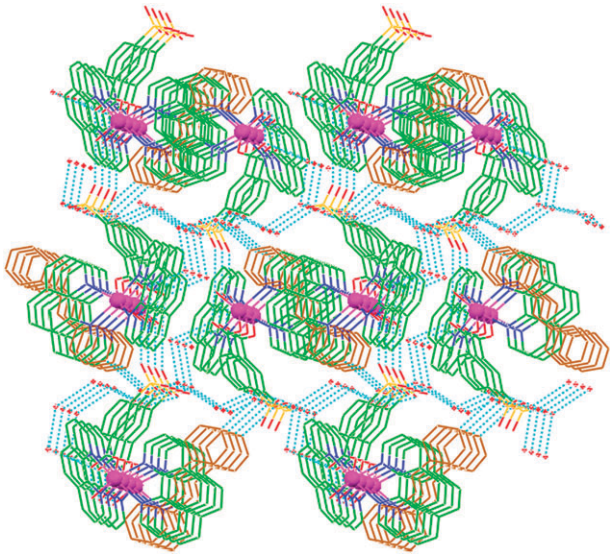

Fig. 17 View of the 3-D hydrogen-bonding network for complex **5**.

charge transfer due to the three coordination or existing modes of the bpe ligands. The absorption peaks of complexes **3** and **4** also come from 4,4′-bipy and phen ligands, and they display similar behavior. The absorption strength of complex **4** is stronger than that of complex **3**, indicating that the coordination of 4,4′-bipy can enhance the absorption. Complexes **5** and **6** also perform similar absorption behavior, and the absorption strength of complex **5** is stronger than that of complex **6**; this may be due to the different hydrogen-bonding forming ability and the stacking interactions of bpe ligands in both complexes.

Catalytic activities

The disproportionation of hydrogen peroxide was selected for the study of the catalytic properties of these six complexes. The H_2O_2 time evolution by monitoring oxygen pressure was measured (Fig. 21). The experiments showed that (1) the base (imidazole, simplified as mz) is an effective assistor for the disproportionation of hydrogen peroxide through the comparison of the blank experiment (kb), kb without mz, **1** without mz, and **3** without mz as shown in Fig. 21; (2) the Mn^{II} complexes can also accelerate the reaction confirmed by the experiments of complexes **1–6**. Results showed that the as-synthesized complex **3** is the most active catalyst for H_2O_2 disproportionation. The essential roles of bases have been mentioned in similar reactions.[20] We confirmed, and believe, that the base helps the subtraction of protons in H_2O_2 molecules, which may help the vicinity of HO_2^- as nucleophilic reagents to the active centers of Mn^{II} catalyst.[21]

Kinetic parameters were obtained from the above experiments and the results showed that the reaction is second order. The best rate equation is $1/p = k/t + b$ (p is the oxygen pressure and the t is time) and the plot is given in Fig. 22. All parameters involved in the reactions are listed in Table 8.

Conclusion

In summary, we have successfully obtained six 3-sulfobenzoate Mn^{II} complexes with one or two neutral ligands. Complexes **1** and **2** contain 4,4′-bipy and bpe, respectively. Complexes **3–6** have two neutral ligands, in which one of the ligands is the 1,10-phenanthroline. The phen ligands all chelate to metal centers in complexes **3–6**. Therefore, such a chelating property leads to the reduction of the coordination sites around metal centers, resulting in the non-coordinating mode for bpe ligands in complexes **5** and **6**, and a dimeric linker and

Table 6 Selected bond lengths (Å) and angles (°) in complex **6**

Mn1–O1	2.1403(15)	Mn1–O6	2.1184(16)
Mn1–N1	2.2716(18)	Mn1–N2	2.2568(18)
Mn1–N3	2.3343(18)	Mn1–N4	2.2575(19)
O1–Mn1–O6	86.12(6)	O1–Mn1–N1	112.90(7)
O1–Mn1–N2	84.62(6)	O1–Mn1–N3	161.04(7)
O1–Mn1–N4	89.73(6)	O6–Mn1–N1	94.27(7)
O6–Mn1–N2	159.83(7)	O6–Mn1–N3	93.01(7)
O6–Mn1–N4	104.47(7)	N1–Mn1–N2	73.06(7)
N1–Mn1–N3	86.05(7)	N1–Mn1–N4	151.67(7)
N2–Mn1–N3	101.48(6)	N2–Mn1–N4	93.37(7)
N3–Mn1–N4	72.13(7)		

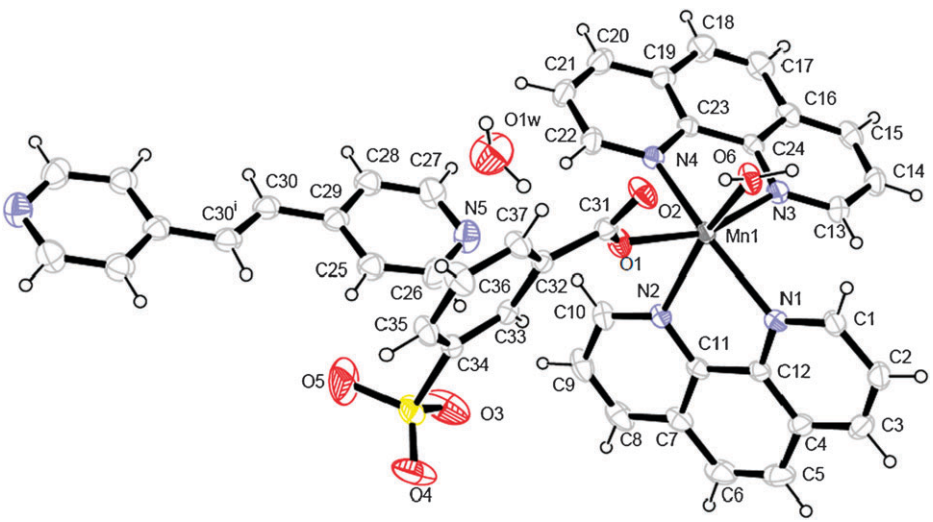

Fig. 18 View of the molecular structure of complex **6**. The thermal ellipsoids are drawn at 30% probability. Symmetry code: $i = 1 - x, -y, -z$.

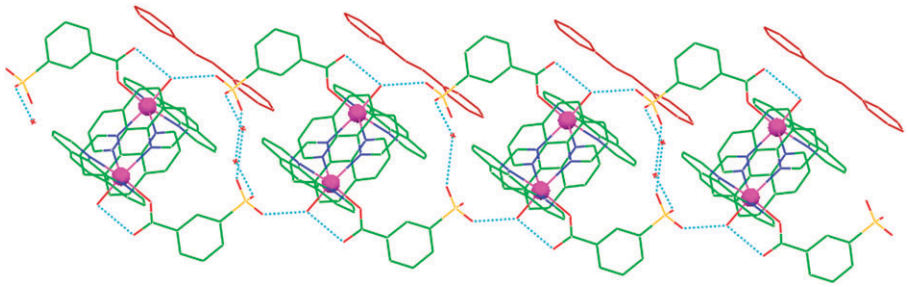

Fig. 19 View of 1-D hydrogen-bonding chain for complex **6**.

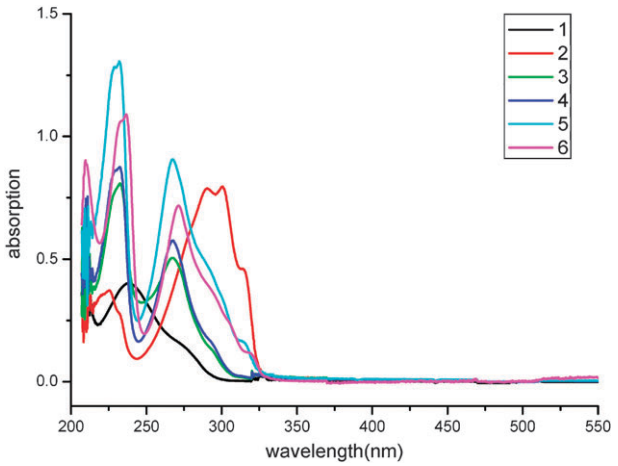

Fig. 20 View of the UV-vis spectra of complexes **1–6** in methanol.

non-coordinating mode for 4,4′-bipy ligands in complexes **3** and **4**. Thus, the hydrogen-bonding forming ability, π–π stacking interactions, and supramolecular assembly in complexes **3–6** are largely different under the adjustment of the phen ligands. The diverse assembly structures lead to the difference in thermal stability, emission properties, absorption behavior, and catalytic activity for the disproportionation of H_2O_2.

Experimental

Materials and physical techniques

All chemicals and solvents used in this study were commercially obtained without further purification. The IR spectra were measured on a Nicolet Nexus 470 spectrophotometer in the 400–4000 cm^{-1} region in KBr pellet. Elemental analyses for C, H, and N were carried out on a ThermoFinnigan Flash EA1112. Thermogravimetric analysis (TGA) was performed by a Delta Series TA-SDT Q600 in a N_2 atmosphere with a heating rate of 10 °C min^{-1} using Al_2O_3 crucibles. The fluorescence study was carried out on a powder sample at room temperature using a Shimadzu RF-50 spectrometer. The electronic spectra were measured on a SPECORD 2000 UV-vis spectrophotometer in the methanol at room temperature.

Synthesis

$[Mn(4,4'\text{-bipy})_2(H_2O)_4](3\text{-sb})\cdot 3H_2O$ (1). A mixture of $Mn(CH_3COO)_2\cdot 4H_2O$ (0.5 mM, 0.123 g), 3-sulfobenzoate monosodium acid (0.5 mM, 0.113 g), 4,4′-bipyridine (0.5 mM, 0.078 g), and H_2O (15 ml) was heated at 433 K in a 30 ml Teflon-lined stainless steel autoclave for 58.5 h. After cooling, a colorless solution was obtained and evaporated at room temperature. A week later, light yellow needle-shaped crystals were precipitated. Yield: 67.0%. Elem. Anal. Calcd for **1**: C, 46.76%; H, 4.94%; N, 8.08%. Found: C, 46.52%; H, 5.01%; N, 7.89%. IR (KBr pellet, cm^{-1}): 3385(vs), 1599(vs), 1559(m), 1535(s), 1490(m), 1415(m), 1374(m), 1215(m), 1182(m), 1087(w), 1067(w), 1032(m), 1002(w), 809(s), 775(w), 667(w), 624(s).

$\{[Mn(3\text{-sb})(bpe)_{1.5}(H_2O)_2](bpe)_{0.5}\cdot H_2O\}_n$ (2). $Mn(CH_3COO)_2\cdot 4H_2O$ (0.5 mM, 0.124 g), 3-sulfobenzoate monosodium acid (0.3 mM, 0.068 g), 1,2-bis(4-pyridine)ethylene (0.2 mM, 0.036 g), and H_2O (10 ml) were mixed in a 20 ml Teflon-lined stainless steel autoclave. The mixture then was heated at 423 K for 72 h. After cooling, a light yellow solution was obtained and evaporated at room temperature. After one week, light yellow crystals were precipitated. Yield: 47.0%. Elem. Anal. Calcd for **2**: C, 55.28%; H, 4.49%; N, 8.32%. Found: C, 55.26%; H, 4.63%; N, 8.28%. IR (KBr pellet, cm^{-1}): 3398(s), 1608(vs), 1573(m), 1560(m), 1426(s), 1397(s), 1220(s), 1189(s), 1104(w), 1035(s), 1014(w), 998(w), 828(m), 765(m), 688(w), 667(m), 618(m), 553(s).

$[Mn(3\text{-sb})(phen)(H_2O)_3](4,4'\text{-bipy})\cdot H_2O$ (3). $Mn(CH_3COO)_2\cdot 4H_2O$ (0.5 mM, 0.123 g), 3-sulfobenzoate monosodium acid (0.5 mM, 0.113 g) and 4,4′-bipyridine (0.5 mM, 0.078 g) were added to a mixed solution of H_2O (15 ml), ethanol (5 ml), and DMF (5 ml) in a 100 ml flask. The mixture solution was refluxed for 2 h, and then phenanthroline (0.5 mM, 0.100 g) was added with further 15 min reflux. After filtration, the solution was evaporated at room temperature. A week later, light yellow block shaped crystals were separated. Yield: 52%. Elem. Anal. Calcd for **3**: C, 52.49%; H, 4.25%; N, 8.44%. Found: C, 52.49%; H, 4.47%; N, 8.43%. IR (KBr pellet, cm^{-1}): 3369(vs), 1624(w), 1594(vs), 1555(s), 1518(m), 1426(s), 1392(vs), 1344(w), 1203(vs), 1146(m), 1093(m), 1063(w), 1034(s), 998(w), 864(w), 850(m), 810(m), 772(m), 752(w), 730(m), 698(w), 668(m), 618(s).

$[Mn_2(3\text{-sb})_2(phen)_2(4,4'\text{-bipy})(H_2O)_4]$ (4). A mixture of $Mn(CH_3COO)_2\cdot 4H_2O$ (0.5 mM, 0.123 g), 3-sulfobenzoate monosodium acid (0.5 mM, 0.112 g), 4,4′-bipyridine (0.5 mM, 0.078 g), and H_2O (15 ml) was heated at 433 K in a 30 ml Teflon-lined stainless steel autoclave for 72 h. After cooling, phenanthroline (0.5 mM, 0.100 g) in DMF (5 ml) was added to the filtration. About one week later, light yellow block-shaped crystals were precipitated. Yield: 43%. Elem. Anal. Calcd for **4**: C, 52.46%; H, 3.67%; N, 7.65%. Found: C, 52.50%;

Table 7 UV-Vis absorption in methanol for complexes **1–6**

Complex	λ_{max}/nm (ε/dm^3 mol^{-1} cm^{-1})			
1	239.6 (33 317)	235.8 (32 976)		
2	314.0 (40 465)	301.6 (68 974)	290.4 (69 123)	225.6 (32 702)
3	267.2 (43 734)	232.4 (69 801)		
4	267.4 (49 330)	232.4 (75 082)	228.4(73 322)	
5	267.6 (75 977)	232.0 (109 505)	228.4 (73 322)	
6	271.4 (63 366)	236.6 (96 272)	233.4 (93 905)	210.4 (78 189)

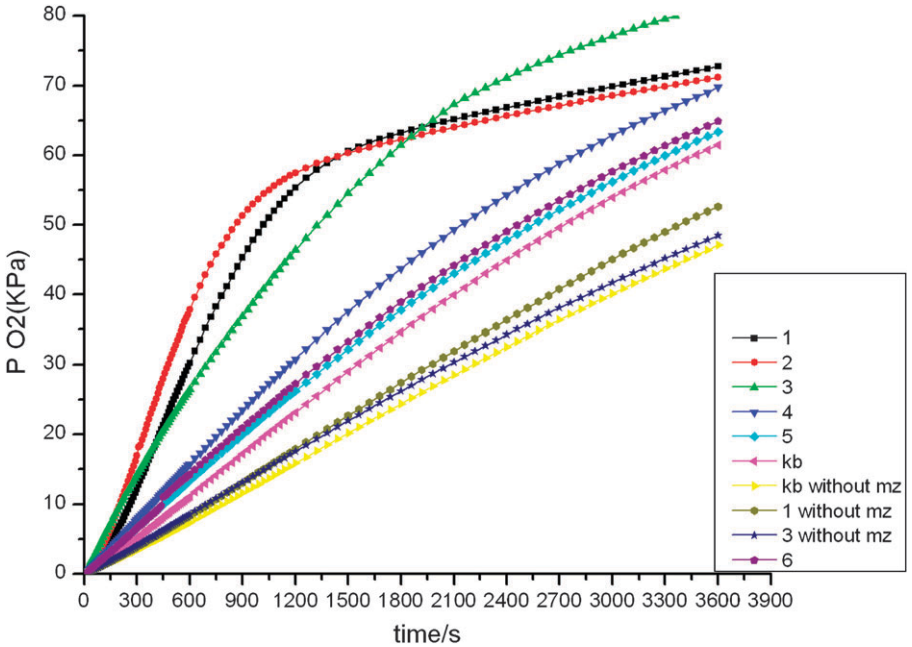

Fig. 21 View of the catalytic behavior for complexes **1–6**. The kb line for blank experiment, kb without mz is the blank experiment without imidazole, **1** without mz and **3** without mz are termed as complexes **1** and **3** used without imidazole, respectively.

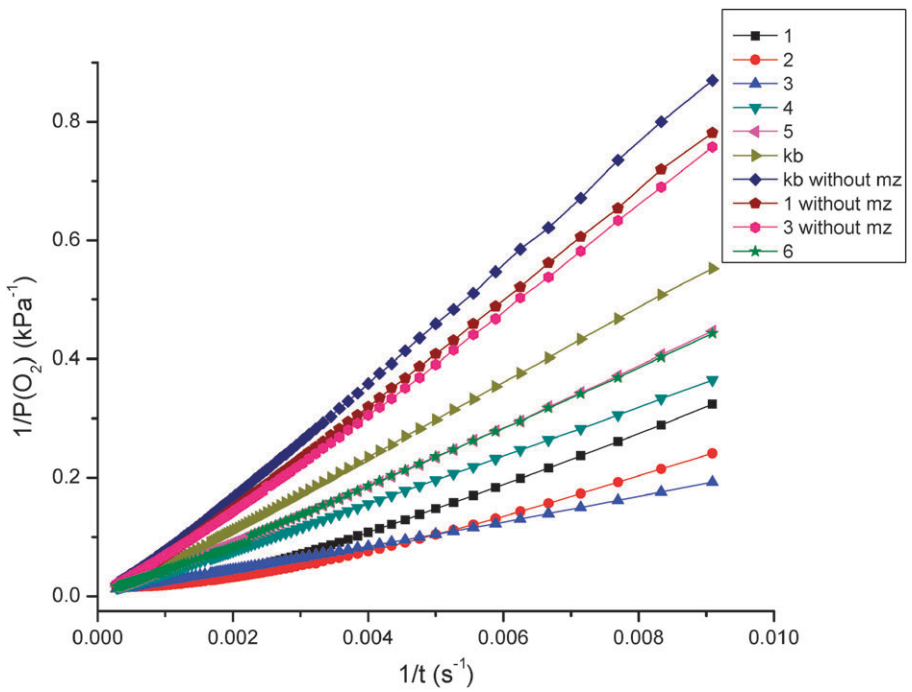

Fig. 22 The plot of $1/p$ *vs.* $1/t$ for complexes **1–6**. The kb line for blank experiment, kb without mz is the blank experiment without imidazole, **1** without mz and **3** without mz are termed as complexes **1** and **3** used without imidazole, respectively.

H, 3.64%; N, 7.66%. IR (KBr pellet, cm^{-1}): 3314(vs), 1672(w), 1651(w), 1606(s), 1592(s), 1557(w), 1516(s), 1493(w), 1424(vs), 1393(vs), 1344(w), 1210(s), 1190(vs), 1165(s), 1094(s), 1077(m), 1033(s), 997(m), 958(w), 923(w), 856(s), 801(m), 772(s), 730(s), 689(m), 666(s), 613(s).

[Mn(3-sb)(phen)$_2$(H$_2$O)](bpe)$_{0.5}$·5H$_2$O (5). Mn(CH$_3$COO)$_2$·4H$_2$O (0.5 mM, 0.123 g), 3-sulfobenzoate monosodium acid (0.5 mM, 0.112 g), 1,2-bis(4-pyridine)ethylene (0.5 mM, 0.091 g), and mixed solvents of H$_2$O–EtOH–DMF (30 ml, volume ratio = 4 : 1 : 1) were mixed in a 100 ml flask, and refluxed for 2 h. Then, phenanthroline (0.5 mM, 0.100 g) in DMF (5 ml) was added with further 15 min reflux. After filtration, the solution was evaporated at room temperature. After two weeks, light yellow block-shaped crystals were grown. Yield: 41%. Elem. Anal. Calcd for **5**: C, 55.55%; H, 4.58%; N, 8.60%. Found: C, 55.55%; H, 4.54%; N, 8.55%. IR (KBr pellet, cm^{-1}): 3416(vs), 1624(m), 1598(vs), 1556(m), 1517(s), 1425(vs), 1384(vs), 1344(w), 1221(s), 1191(vs), 1142(w), 1095(m), 1034(s), 999(w), 847(m), 828(w), 770(m), 726(vs), 689(m), 665(m), 617(vs), 556(m).

[Mn(3-Sb)(phen)$_2$(H$_2$O)](bpe)$_{0.5}$·H$_2$O (6). A mixture of Mn(CH$_3$COO)$_2$·4H$_2$O (0.5 mM, 0.123 g), 3-sulfobenzoate monosodium acid (0.5 mM, 0.112 g), 1,2-bis(4-pyridine)ethylene (0.4 mM, 0.073 g), and H$_2$O (15 ml) was sealed in a 30 ml Teflon-lined stainless steel autoclave and heated at 423 K for 3 d. After cooling, phenanthroline (0.8 mM, 0.160 g) in DMF (5 ml) was added and evaporated at room temperature. Several days later, light yellow block-shaped crystals were grown. Yield: 45.0%. Elem. Anal. Calcd for **6**: C, 59.84%; H, 3.94%; N, 9.43%. Found: C, 59.67%; H, 4.04%; N, 9.06%. IR (KBr pellet, cm^{-1}): 3537(vs), 3469(vs), 1624(m), 1593(s), 1555(m), 1516(s), 1425(s), 1381(vs), 1341(w), 1230(s), 1185(s), 1163(m), 1142(w), 1092(m), 1078(w), 1034(s), 995(w), 850(m), 835(m), 771(m), 724(s), 687(w), 662(m), 615(s), 559(m).

Table 8 The kinetic parameters in catalytic reactions for complexes **1–6**

Complexes	k	Equation
1	31.70	$1/p = 31.70/t + 0.0096$
2	22.23	$1/p = 22.23/t + 0.0030$
3	20.01	$1/p = 20.01/t + 0.0050$
4	39.22	$1/p = 39.22/t + 0.00018$
5	47.56	$1/p = 47.56/t + 0.0018$
kb	60.66	$1/p = 60.66/t + 0.0068$
kb without mz	94.91	$1/p = 94.91/t + 0.016$
1 without mz	85.04	$1/p = 85.04/t + 0.015$
3 without mz	81.14	$1/p = 81.14/t + 0.012$
6	47.58	$1/p = 47.58/t + 0.0036$

X-Ray structure determination

Data collections were performed on a Bruker SMART diffractometer equipped with a CCD area detector. The data were integrated by use of the SAINT program,[22] with the intensities corrected for Lorentz factor polarization and absorption. The structures were solved by direct methods and successive Fourier syntheses. Full-matrix least square refinements on F^2 were carried out using SHELXL-97 package.[23] All non-hydrogen atoms were anisotropically refined. Atom O3w in complex **1** is disordered over two positions. The sulfonate groups in complexes **5** and **6** are disordered. Hydrogen atoms on carbon atoms were placed in idealized positions and refined as riding atoms, with C–H = 0.93 Å and U_{iso}(H) = 1.2U_{eq}(C). H atoms on water molecules in **1**, **2**, **3**, **4**, and **6** were found in the Fourier maps and refined with

Table 9 Crystallographic data and refinement parameters for complexes **1–6**

Complex	**1**	**2**	**3**	**4**	**5**	**6**
Formula	$C_{27}H_{34}MnN_4O_{12}S$	$C_{31}H_{30}MnN_4O_8S$	$C_{29}H_{28}MnN_4O_9S$	$C_{24}H_{20}MnN_3O_7S$	$C_{37}H_{37}MnN_5O_{10}S$	$C_{37}H_{29}MnN_5O_7S$
Mr	693.58	673.60	663.56	549.44	798.73	742.67
Crystal color/shape	Yellow/needle	Yellow/block	Yellow/block	Yellow/block	Yellow/block	Yellow/block
Crystal size/mm	0.38 × 0.17 × 0.10	0.32 × 0.23 × 0.22	0.35 × 0.30 × 0.15	0.30 × 0.28 × 0.12	0.16 × 0.12 × 0.10	0.38 × 0.14 × 0.14
Space group	Monoclinic, $P2_1/c$	Triclinic, $P\bar{1}$	Monoclinic, $P2_1$	Monoclinic, $P2_1/c$	Monoclinic, $P2_1/c$	Triclinic, $P\bar{1}$
a/Å	20.510(2)	11.7416(10)	7.4415(8)	13.7428(15)	11.5735(8)	10.7849(15)
b/Å	7.0178(8)	11.9663(10)	20.268(2)	13.7074(15)	14.5456(10)	11.3475(16)
c/Å	23.495(3)	12.9264(11)	10.2404(11)	14.2123(15)	22.7033(15)	14.816(2)
α°	90.0	69.042(1)	90.0	90.0	90.0	100.909(1)
β°	112.446(1)	89.555(1)	107.609(1)	118.334(1)	104.600(1)	97.804(1)
γ°	90.0	67.904(1)	90.0	90.0	90.0	109.911(1)
V/Å^3	3125.6(6)	1554.5(2)	1472.1(3)	2356.5(4)	3698.6(4)	1634.2(4)
Z	4	2	2	2	4	2
D/g cm^{-3}	1.470	1.439	1.497	1.549	1.434	1.509
T/K	295 ± 2	295 ± 2	295 ± 2	295 ± 2	295 ± 2	295 ± 2
μ/mm^{-1}	0.557	0.549	0.581	0.700	0.478	0.529
θ range/°	1.1–25.2	1.7–25.2	2.0–25.2	1.7–25.2	1.7–25.2	1.4–25.2
Measured reflections	22 010	11 460	9285	13 083	18 967	12 170
Unique reflections	5629	5549	5193	4204	6658	5822
Observed reflections	3969	5153	4907	3516	4738	4817
F(000)	1444	698	686	1128	1660	766
R_1 and wR_2 ($I > 2\sigma(I)$)	0.055, 0.141	0.061, 0.129	0.033, 0.073	0.038, 0.090	0.064, 0.152	0.039, 0.095
R_1 and wR_2 (all data)	0.080, 0.157	0.066, 0.132	0.035, 0.074	0.047, 0.095	0.090, 0.166	0.049, 0.100
Number of variables	455	424	421	341	560	499
GOF	0.991	1.139	1.032	1.027	1.127	1.067
Largest difference peak and hole/e Å^{-3}	0.859, −0.529	0.658, −0.487	0.225, −0.254	0.282, −0.273	0.669, −0.223	0.452, −0.265

restriction geometries. H atoms on lattice water molecules in **5** were not added as these water oxygens have large U_{eq} values. All the programs used are included in the WinGX Suite with the version of 1.64.[24] The molecular drawings were helped by the ORTEP-III for Windows[25] and Mercury software.[26] Detail crystal data and structure refinements for **1–6** are listed in Table 9.

Hydrogen peroxide disproportionation study

A mixture of water (5 mL), imidazole (aqueous solution with 0.1 mol L^{-1}), and DMSO (1 mL) containing an as-synthesized complex (in the blank experiment this material was not added) with a concentration of 0.59×10^{-3} mol L^{-1} in a three-necked flask of 100 mL was stirred in a thermostated cell at 14 °C. Three experiments were in the absence of imidazole and 1 mL water was added (Fig. 21). The flask was connected with a pump and a pressure gauge (APM-2D), respectively. With a vacuum pump, an average 2.0 kPa pressure above the solution was obtained and kept. Then zero setting was done. At this moment, hydrogen peroxide (1 ml; H_2O_2 30% w/w) was introduced into the system by a syringe and immediately the time and the evolved oxygen pressure were recorded.

Acknowledgements

The authors thank the National Natural Science Foundation of China (grant No. 50073019).

References

1 S. R. Batten and K. S. Murray, *Coord. Chem. Rev.*, 2003, **246**, 103.
2 K. Biradha, M. Sarkar and L. Rajput, *Chem. Commun.*, 2006, 4169.
3 N. R. Champness and M. Schroder, *Curr. Opin. Solid State Mater. Sci.*, 1998, **3**, 419.
4 (*a*) S. Kitagawa, R. Kitaura and S. Noro, *Angew. Chem., Int. Ed.*, 2004, **43**, 2334; (*b*) S. Kitagawa and M. Kondo, *Bull. Chem. Soc. Jpn.*, 1998, **71**, 1739.
5 G. Marinescu, M. Andruh, M. Julve, F. Lloret, R. Llusar, S. Uriel and J. Vaissermann, *Cryst. Growth Des.*, 2005, **5**, 261.
6 L. G. Zhu and S. Kitagawa, *Inorg. Chem. Commun.*, 2003, **6**, 1051.
7 (*a*) S. Mukhopadhyay, P. B. Chatterjee, D. Mandal, G. Mostafa, A. Caneschi, J. van Slageren, T. J. R. Weakley and M. Chaudhury, *Inorg. Chem.*, 2004, **43**, 3413; (*b*) C. Y. Chen, P. P. Chu and K. H. Lii, *Chem. Commun.*, 1999, 1473.
8 (*a*) W. S. Han and S. W. Lee, *Dalton Trans.*, 2004, 1656; (*b*) T. J. R. Weakley, *Inorg. Chim. Acta*, 1982, **63**, 161; (*c*) M. Bukowska-Strzyzewska and A. Tosik, *Acta Crystallogr., Sect. B: Struct. Crystallogr. Cryst. Chem.*, 1982, **38**, 265; (*d*) J. Tao, X. Yin, Z. B. Wei, R. B. Huang and L. S. Zheng, *Eur. J. Inorg. Chem.*, 2004, 125; (*e*) P. Q. Zheng, L. S. Long, R. B. Huang and L. S. Zheng, *Appl. Organomet. Chem.*, 2003, **17**, 739.
9 (*a*) L. P. Zhang and L. G. Zhu, *CrystEngComm*, 2006, **8**, 815; (*b*) X. F. Zheng and L. G. Zhu, *Cryst. Growth Des.*, 2009, **9**, 4407.
10 L. P. Zhang and L. G. Zhu, *Acta Crystallogr., Sect. E: Struct. Rep. Online*, 2005, **61**, m1264.
11 L. P. Zhang and L. G. Zhu, *Z. Anorg. Allg. Chem.*, 2008, **634**, 39.
12 L. F. Ma, J. Q. Liu and L. Y. Wang, *Synth. Rea. Inorg. Mnet.-Org. Nano-Met. Chem.*, 2007, **37**, 501.
13 H. P. Xiao, X. H. Li and M. L. Hu, *Acta Crystallogr., Sect. E: Struct. Rep. Online*, 2005, **61**, 506.
14 S. T. Castaman, S. Nakagaki, R. R. Ribeiro, K. J. Ciuffi and S. M. Drechsel, *J. Mol. Catal. A: Chem.*, 2009, **300**, 89.
15 M. M. Heravi, H. A. Oskooie, R. Malakooti, B. Alimadadi, H. Alinejad and F. Behbahani, *Catal. Commun.*, 2009, **10**, 819.
16 M. Montazerozohori, M. H. Habibi, L. Zamani-Fradonbe and S. A. R. Musavi, *Arkivoc*, 2008, 238.
17 (*a*) M. L. Tong, H. K. Lee, X. M. Chen, R. B. Huang and T. C. W. Mak, *J. Chem. Soc., Dalton Trans.*, 1999, 3657; (*b*) R. H. Wang, F. L. Jiang, Y. F. Zhou, L. Han and M. C. Hong, *Inorg. Chim. Acta*, 2005, **358**, 545; (*c*) S. F. Lu, Y. B. Zhu, Y. C. Liang, R. M. Yu, X. Y. Huang, F. X. Sun, Q. J. Wu and Z. X. Huang, *Acta Chim. Sinica*, 2004, **62**, 253.
18 X. H. Miao and L. G. Zhu, *Z. Anorg. Allg. Chem.*, 2008, **634**, 335.
19 A. Vogler and H. Kunkely, *Coord. Chem. Rev.*, 2007, **251**, 577.
20 M. Devereux, M. McCann, V. Leon, V. McKee and R. J. Ball, *Polyhedron*, 2002, **21**, 1063.
21 V. Viossat, P. Lemoine, E. Dayan, N. H. Dung and B. Viossat, *Polyhedron*, 2003, **22**, 1461.
22 G. M. Sheldrick, *SADABS, Program for area detector adsorption correction*, Institute for Inorganic Chemistry, University of Göttingen, Germany, 1996.
23 G. M. Sheldrick, *SHELXL-97, Program for refinement of crystal structures*, University of Göttingen, Germany, 1997.
24 L. J. Farrugia, *WINGX: A windows program for crystal structure analysis*, University of Glasgow, Great Britain, 1998.
25 L. J. Farrugia, *J. Appl. Crystallogr.*, 1997, **30**, 565.
26 C. F. Macrae, P. R. Edgington, P. McCabe, E. Pidcock, G. P. Shields, R. Taylor, M. Towler and J. van de Streek, *J. Appl. Crystallogr.*, 2006, **39**, 453.

